WSEAS TRANSACTIONS on SYSTEMS

Cannizzaro L., Virzi' Mariotti G.,
Giallanza A., Porretto M., Marannano G.

Study of a Semi Active Electromagnetic Regenerative Suspension

CANNIZZARO L., VIRZI' MARIOTTI G., GIALLANZA A., PORRETTO M., MARANNANO G.
Department of Industrial and Digital Innovation - Chemical, Management, Computer Science and
Mechanical Engineering
University of Palermo
Viale delle Scienze - 90128 Palermo
ITALY
luigi.cannizzaro@unipa.it gabriele.virzimariotti@unipa.it antonio.giallanza@unipa.it
marioporretto.im@gmail.com giuseppe.marannano@unipa.it

Abstract: The main objective of this work is the theoretical and numerical study of a device that allows recovering energy from an automobile suspension. In place of the viscous damper, which dissipates the kinetic energy of the vehicle due to rough roads or more marked obstacles, an electromagnetic damper performs the functions of the viscous shock absorber with a recovery of electric energy. The damper has permanent magnets and its working is based on the electromagnetic induction. The used ferromagnetic material is the Supermendur, which has very good ferromagnetic properties, but is expensive and difficult to found, so that the choice of different material is useful to reduce the costs. The mathematical model describes the operation of the damper, restoring the values of the electrical and mechanical magnitudes versus the relative speed between the stem and the stator. Several finite element analyses, conducted in ANSYS Workbench Magnetostatic, confirm both the magnetic field and flux values obtained through the theoretical analysis. A calculation example of the energy recovery is done considering an electric minicar transiting on a bumpy road (IRI=3); the recovered power has a total value of 280W about; at last a comparison with similar devices proves the excellent quality of the design also if the comparison should be done with uniformity of the parameters.

Key-Words: -Suspension; Regenerative damper; Energy harvesting; Electromagnetic shock absorber; FE analysis.

1 Introduction

In the last years, automotive research aims to maximize the passengers comfort and the efficiency of all vehicle components. The energy losses have to be minimized, especially in hybrid vehicles, by recovering energy from all the installed devices. The kinetic energy is commonly dissipated into heat in the case of brakes or suspensions. The amount of recoverable braking energy is much higher than the energy obtained by a suspensions system. However, many studies are found regarding the possibility of energy harvesting by the vehicles suspensions using electromagnetic dampers, which have to be compact and efficient. For this reason, almost all solutions of electromagnetic dampers are based on the use of rare-earth permanent magnets. The electromagnetic dampers are not only used in automotive field, but even in civil structures in order to damp the vibrations and thereby reduce or eliminate the noise. The wind or even the earthquakes produce vibrations that may be damped in order to recover the energy. Some authors have proposed different types of electromagnetic dampers. In [1] and [2] these are based on rotary actuators requiring a motion converter involving many complexities.

Cassidy et al. [3] studied an electromagnetic device for energy harvesting from civil structures based on the conversion, by means of a ball-screw mechanism, of the linear motion in rotating motion. The same solution is adopted by Amati et al. [4] that use a ball screw mechanism to design an electromagnetic damper for automotive applications. Several Authors [5] [6] [7] [8] [9] [10] [11] [12] designed and studied similar solutions. The work [8] studies a new zero active suspension that combines the advantages of active and semi-active systems. Yin et al. [13] compare a damper with ball screw mechanism and a damper constituted by a gearbox and an electric generator. Authors state that a damper constituted by gearbox introduces a significant unsprung mass due to the inertia of the rotating components of the device. Li et al. [14] propose the design, bench experiments and road tests of a retrofit regenerative shock absorber based on a permanent magnetic generator and a rack–pinion mechanism. Results show that variable damping coefficient and the asymmetric feature in jounce and rebound motions are achieved by controlling the electrical load of the shock absorber. Suda et al. [15] [16] present a method to

WSEAS TRANSACTIONS on SYSTEMS

Cannizzaro L., Virzi' Mariotti G.,
Giallanza A., Porretto M., Marannano G.

solve the problems in active and passive control systems: in passive suspension an energy regenerative damper system converting vibrations into useful energy is proposed. The hybrid system combines this energy regenerative system and active control in order to achieve good performance of vibrations reduction with little energy consumption. Nakano [17] applies the system in a truck cabin suspension. Another important application of regenerative damper is related to renewable energy production. In fact, dampers are used to recovery energy from the sea wave motion [18] [19] [20]. As already mentioned, the use of ball screw mechanism inevitably reduces the device efficiency. Moreover, the rotor inertia of the rotating generator could have effects on the suspension behavior. For this reason, many studies have the aim to design linear electromagnetic regenerative shock absorbers, which may have several configurations; therefore the use of rare-earth permanent magnets that produce a strong magnetic field is strictly necessary. On the other hand, the configuration of the stator coils can be varied in order to investigate the better solution in terms of damping coefficient, stability and efficiency. More frequently studied configurations have the coils arranged with their axis aligned with the magnets axis and with the damper axis [21] [22] [23] [24]. Oprea et al. [21] analyze an electromagnetic damper optimizing the device configuration by means of finite element analysis. They correctly affirm that the rod supporting the magnets and spacers should be highly reluctant but they do not specify the used material. Nagode et al. [22] study two types of electromagnetic dampers for railroad applications and implement a prototype. Zuo et al. [10] [23] design and carry out analysis on a retrofit regenerative shock absorber. The wave form of the regenerated currents is much irregular and for this reason [23] the Authors study a circuit in order to correct the power output. Tang et al. [24] design and optimize a tubular linear electromagnetic damper consisting of an aluminum rod with axial magnets and spacers. They optimize the thickness of magnets and spacers to obtain the maximum power density; they analyze a new configuration of magnets and coils and compared the results. Moreover, in [25], Authors use the optimal size of magnets and spacers and, at last, carry out a thermal analysis. In the paper [26] two configurations of regenerative electromagnetic shock absorbers are developed: a linear device and a rotary device. Performance of these shocks in a laboratory test stand and in a small all-terrain vehicle is described. The paper [27] shows that the magnetic damper system using a

phase lead controller is excellent in reducing the vibration of a one degree of freedom suspension. Another device, which is alternative to electromagnetic damper, is the magnetorheological one; the application is based on substances with ferromagnetic powder that change their viscosity if immersed in a magnetic field. Energy recovered by the generator from the mechanical sub-system is partly converted into heat in the generator windings, while MR dampers utilise the remaining part; in some case [28] they need a control system for their application. Many papers are found in the literature on this scope, see for example [29] [30] [31].

In this work, Authors study an innovative electromagnetic damper consisting of a stainless steel rod having a great reluctance and a greater mechanical strength than the aluminum alloy rod used in [21]. The main difference consists in a new disposition of the coils with respect to other literature studies; in fact, the axis of each coil is perpendicular to the damper axis. The magnets are stacked with reverse magnetization axis [32] [33] [34], in order to direct the magnetic flux toward the spacers (which have great magnetic permeability) and, finally, toward the coils. The mathematical model of the damper is defined considering the variable inductance of the coils with the movement of the stem. In fact the magnetic circuit reluctance is variable because the thickness of the air gap varies during the stem displacement. The mathematical model is implemented in Matlab Simulink environment in order to characterize the device operating. FE analysis, using Ansys Workbench Magnetostatic, is used to verify the magnetic flux density, previously calculated analytically. Finally, the damping coefficient and the energy harvesting potential are evaluated considering that the connection to a harvesting system produces substantial variations in the suspension behavior.

2 Geometry and magnetic flux determination

The studied device is constituted by a sliding and a stator; this consists in a ferromagnetic cylindrical part with some slots to place the electromagnetic coils. The stroke of the damper is equal to 207 mm, the stator outer diameter is equal to 66 mm, and 100 mm in the section where the coils are placed (Fig.1). The slots allow placing 20 coils, positioned in order to synchronize their effect, in terms of force on the stem. Fig 1(a) shows the longitudinal section of the stator part and the layout of the coils (schematically shown). In particular the coils axes are disposed

WSEAS TRANSACTIONS on SYSTEMS

Cannizzaro L., Virzi' Mariotti G.,
Giallanza A., Porretto M., Marannano G.

perpendicularly to the translation axis of the stem. The tubular part, where the coils are not present, acts as a rail for the stem in order to support possible bending actions. The sliding part (Fig. 1b) is constituted by a stem, where annular rare-earth permanent magnets are placed. The magnets are stacked with alternated magnetization direction and are separated by means of ferromagnetic spacers. This configuration, in accordance with [24], allows maximizing the magnetic flux concatenated with the coils. The diameter of the spacers is slightly lower than the inner diameter of the stator, in order to leave an as small as possible air gap between the stator and translating parts, given that these parts are constantly in relative motion during the working. The movement of the stem produces a magnetic flux variation through the coils. The magnetic circuit of the device cyclically changes: in particular, when the spacer is positioned in correspondence of the coils core (minimum air gap τ=0.5mm) the reluctance of the circuit has the minimum value and the flux lines are optimally directed.
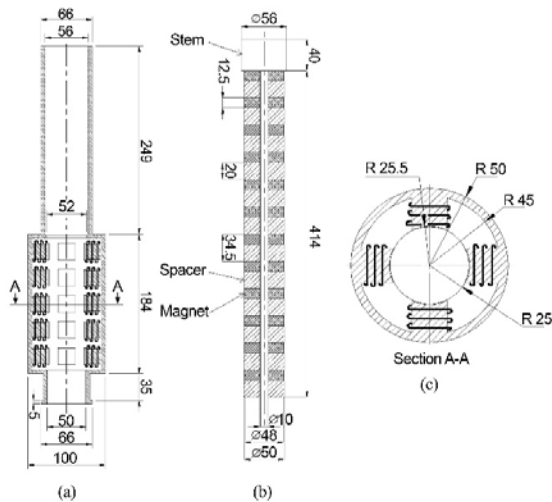

Fig.1: (a) longitudinal section of the stator and (b) sliding part; (c) transversal section of the stator.
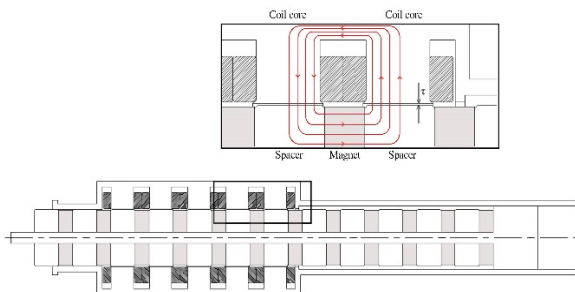

Fig. 2: Damper with the stem in the maximum concatenated flux position.

Fig. 2 shows the damper with the stem in the maximum concatenated flux position. The detail shows the schematic distribution of the flux lines.

When the stem is moved by an amount equal to half the pitch of the spacers (Fig. 3), the opposite situation is established, and the reluctance of the magnetic circuit increases. This is due to the assumed geometric configuration and to the increment of the air gap. The stem position, shown in Fig. 3, leads a concatenated flux approximately equal to zero. The relative detail shows the main schematic distribution of the flux lines; the flux lines form closed rings around the coil core. The magnetic flux is much lower than the case of Fig. 2 because it is equal to: $\phi = \int B\hat{n}d\Sigma$ and the unit vector $\hat{n}$ has perpendicular direction to the concatenation section of the coil.
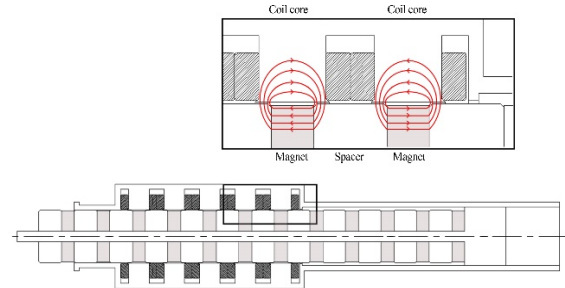

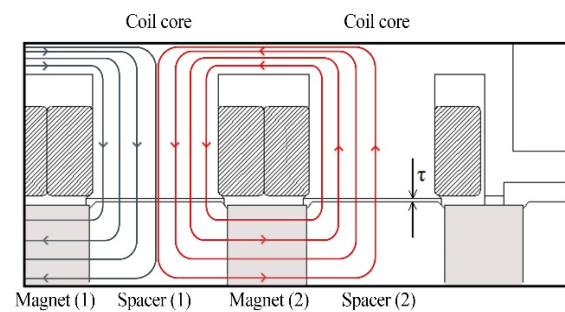Fig. 3: Damper with the stem in the position of minimum concatenated flux.

Fig. 4: Detail of the stem in the position of maximum concatenated flux.

When the stem is located in the maximum flux position (each spacer is aligned with the four radial coils, Fig. 1c), the surfaces involved by the magnetic flux are the lateral surface of the spacer and the four surfaces of the stator coils cores (Fig. 4). The ferromagnetic cores and the spacers are crossed by equally oriented flux lines that are generated from consecutive magnets with opposite magnetization orientations; moreover, the flux crosses a magnetic circuit with two air gaps. Fig. 4 shows also that the magnet (2) flux red lines pass counterclockwise through the spacer (2), the first air gap, the cores of the stator coils, the second air gap and, finally, the spacer (1) and then close on the permanent magnet.

WSEAS TRANSACTIONS on SYSTEMS

Cannizzaro L., Virzi' Mariotti G.,
Giallanza A., Porretto M., Marannano G.

2.1 Choice of the materials and determination of the concatenated magnetic flux

Choice of the materials is based on the need to maximize the effect that the permanent magnets have on the stator. The stator material is chosen with a very high magnetic permeability, in order to maximize the concatenated magnetic flux. Very attention has to be put also to the shape of the hysteresis cycle: a material with a very broad hysteresis cycle is named *hard magnetic,* since it must be subjected to a very high magnetic field (materials used for permanent magnets) to magnetize or demagnetize it; the materials having a very narrow hysteresis cycle are named *soft magnetic;* they are easily magnetized and do not remain magnetized. The optimal choice of the ferromagnetic material is very difficult, since these materials are very expensive and uncommon, so that cost, workability and availability have to be taken in account. The study of this work does not consider these necessities, and the material is only chosen for the excellent quality of magnetization. Only to illustrate the procedure, a very good material for the stator is "Supermendur" that is used in the electrical machines due to the excellent magnetic quality; since it is expensive and is found with difficulty, the definitive choice is referred to a successive research.
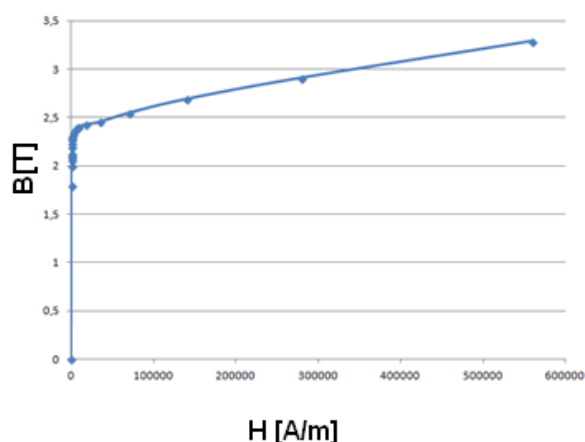

H [A/m]
Fig. 5 – Supermendur B-H characteristic

In general B-H characteristic curve of the ferromagnetic material is defined to describe its real magnetic behavior; the slope of the curve in each point is equal to the value of permeability: $\mu_r = \partial B / \partial H$. To do it, a device called "device (or "yoke") of Epstein" can be used for the industrial evaluation of energy losses, due to hysteresis and eddy currents, which are found in ferromagnetic materials when immersed in a variables magnetic field; the experimental procedure is reported in [35]. Otherwise the literature data (for instance [36]) can be used.

Supermendur is an Iron-Cobalt and Vanadium alloy in the following proportions: 49% Fe – 49% Co – 2% V. Fig. 5 shows its B-H characteristic. The relative magnetic permeability is $\mu_r = 65000 \; Wb/A$; it is constant for this material until an induction $B = 2T$; more than this value the permeability decreases quickly and one has $\mu_r = 3800 \; Wb/A$ for $B = 2.3T$ [36].

Separator rings, interposed among the magnets, are also constituted by such material, because they have the purpose to swerve the flux lines of the magnetic field and to canalize them towards the stator. Instead the stem, where magnets and rings are stacked, cannot be constituted by the same material, because the magnetic field lines produced by the magnets would close on the rod, and the stator would be invested by a very lower flux. The stem is implemented in stainless steel with very high reluctance; in fact the relative permeability $\mu_r = \frac{\mu}{\mu_0}$ is $100 \div 5000$. The magnetic flux concatenated with the stator and the windings is thus maximized.
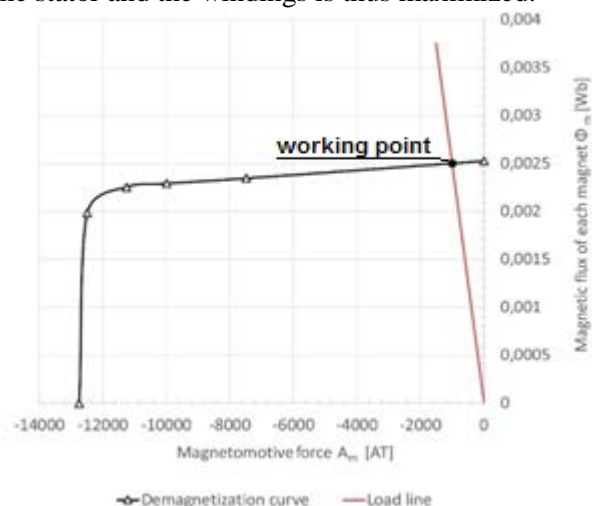

Fig. 6 – Demagnetization curve; working point and determination of the magnetic flux.

A first estimation of the magnetic flux, concatenated with each of the 20 windings, is done analytically, considering the magnetic circuit formed by magnets and stator. Magnetic circuit reluctance is calculated by the reluctances of magnetic gaps only, neglecting the very lower reluctance of Supermendur.
The air gap reluctance is:

$$R_t = \frac{\tau}{\mu_0 \mu_{r\Sigma}} [H^{-1}] \qquad (1)$$

Where τ is the minimum air gap and Σ is the total surface of the windings exposed to the magnetic flux. The total reluctance is given by $2R_t$ since the 2 air gaps are in series. In this hypothesis the working curve of the magnets may be evaluated by the characteristics of the material:

WSEAS TRANSACTIONS on SYSTEMS

Cannizzaro L., Virzi' Mariotti G.,
Giallanza A., Porretto M., Marannano G.

$$\phi_m = -\frac{A_m}{2R_t} \qquad (2)$$

Where A_m is the magnetomotive force. Fig. 6 shows the point of work that is given by the intersection of the characteristic curve of the magnet with the straight line of work of the magnetic circuit, by the relationship (2).

Flux generated by a magnet passing through the magnetic circuit, corresponding to the work point, is equal to $\phi_m = 2.48 \cdot 10^{-3} Wb$. In particular Fig.1(c) and Fig. 4 show that the total magnetic flux is generated by two consecutive magnets and it involves four coils for each considered section. Finally, the flux passing through each coil is obtained by:

$$\phi_c = \frac{2 \cdot \phi_m}{4} = 1.24 \cdot 10^{-3} Wb \qquad (3)$$

This is the maximum generated flux when the stem is positioned with the spacers aligned with the coils cores. The mean electromagnetic induction in each coils cores is obtained by:

$$B_c = \frac{\phi_c}{\Sigma} = 2.43 T \qquad (4)$$

Both the mean induction value and the concatenated flux are compared with the results by finite element analysis, performed in Ansys Workbench Magnetostatic environment. Fig. 7 shows the trend of the magnetic field flux lines.
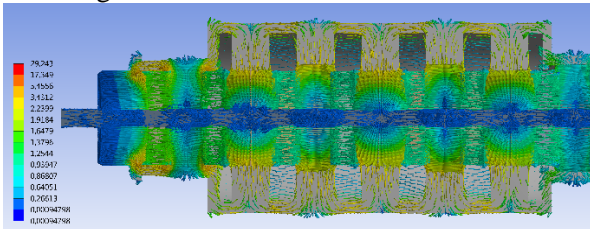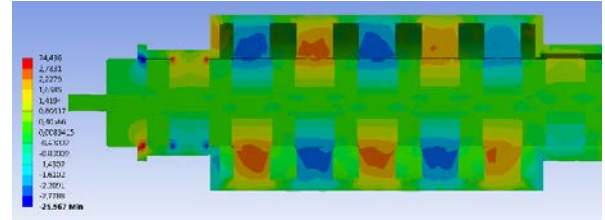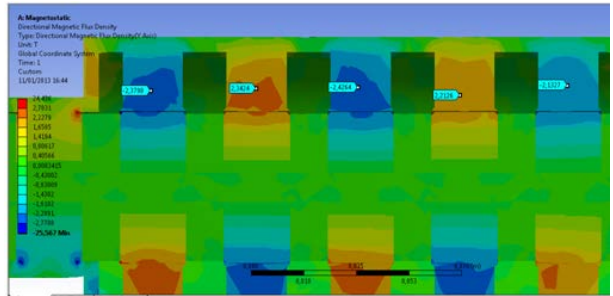

Fig. 7: Magnetic field flux lines (maximum concatenated flux position).

Fig. 8a shows the directional magnetic flux density (value of mean induction calculated along the perpendicular direction to the surface of the coils cores) that allows the flux calculation and the induced electromotive force. Fig. 8b shows the detail with the flux values. The numerical simulation provides a mean induction value on the coils cores, equal to: $B_c^* = 2.3 T$. This value is slightly lower than the analytical study because the ferromagnetic material reluctance is omitted in the FEM analysis. For each coil, the concatenated flux is equal to $\phi_c^* = B_c^* \cdot \Sigma = 1.15 \cdot 10^{-3} Wb$; table 1 summarizes the comparison results. The stem displacement (by an amount equal to the magnets

pitch) provides a concatenated flux variation through coils. Since the magnetization directions are opposite, flux passes from the maximum positive value $\left(\phi_c^*\right)_{max} = 1.15 \cdot 10^{-3} Wb$ to the maximum negative value $\left(\phi_c^*\right)_{min} = -1.15 \cdot 10^{-3} Wb$

(a)

(b)

Fig. 8: Directional magnetic flux density (maximum concatenated flux position).(a) general view; (b) particular with the flux values.
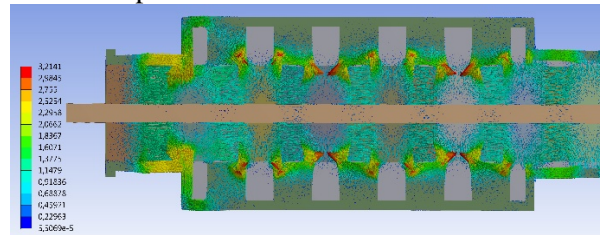

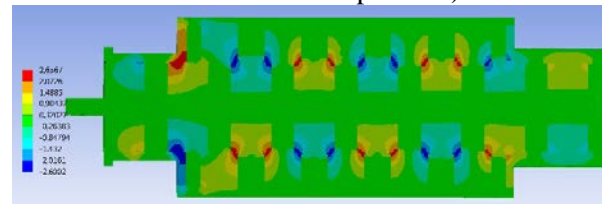Fig. 9: Magnetic field flux lines (minimum concatenated flux position).

Fig. 10: Directional magnetic flux density (minimum concatenated flux position).

Table 1 – analytical-numerical comparison

	Analytical	Numerical
B_c	2.43 T	2.3 T
ϕ_c	1.24 10⁻³ Wb	1.15 10⁻³ Wb

Consequently, for an intermediate position of the stem, the magnetic flux must assume zero value. Fig. 9 shows the results of an analysis performed with the stem shifted of an amount equal to the half-

WSEAS TRANSACTIONS on SYSTEMS

Cannizzaro L., Virzi' Mariotti G.,
Giallanza A., Porretto M., Marannano G.

pitch of the magnets, in the maximum flux position; the flux lines close in on themselves, passing through only a limited part of the stator cores.

Fig. 10 shows that the magnetic flux distribution density provides values near to zero in the direction orthogonal to the surface of the coils. Analysis of directional magnetic flux density gives flux values equal to zero about, in the orthogonal direction to the coils surface, as Fig. 11 shows.

The mean induction value in the direction of the coils axes is equal to $B_c^* = 0.03T$. The mean flux is equal to $\phi_c^* = B_c^* \cdot \Sigma = 2.55 \cdot 10^{-5} Wb$.

Fig. 12 shows the flux variation versus the stem displacement. The graph is obtained by magnetostatic analyses varying the stem position from time to time.
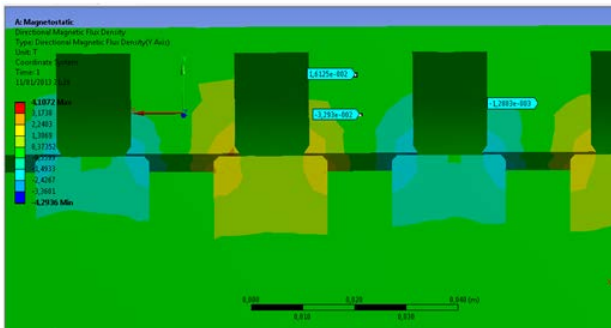

Fig. 11 – Particular of the directional magnetic flux density (intermediate position); flux values are highlighted.
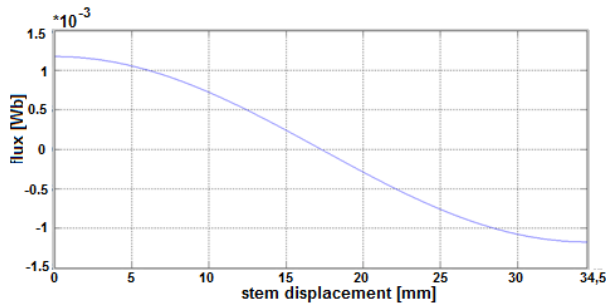

Fig. 12 – Variation of the flux concatenated with one coil for a displacement 2Δs = 34.5 mm that is the pitch of the separation rings.

3 Mathematical model and working analysis

Relative motion between sliding part and the stator generates a magnetic flux variation through coils. Several FE analyses, that are conducted varying the relative position, show that the variation can be well approximated by a sinusoidal law. In particular, Fig. 13(a) and 13(b) respectively show the flux and the inductance variation of each coil versus the stem
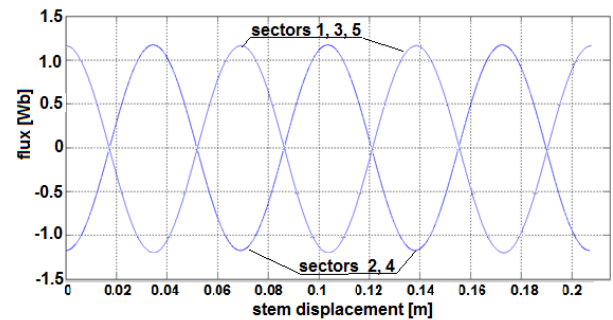
displacement. The inductance is related to the stem movement that causes the reluctance variation.

The electromotive force expression in each coil can be analytically determined by:

$$\varepsilon_i(x) = -N\frac{d\Phi(x)}{dx}V_s = -N\left[-\phi(x)_{\max}\frac{\pi}{p}\sin\left(\frac{\pi}{p}x\right)\right]\omega\frac{C}{2}\sin(\omega t) \quad (5)$$
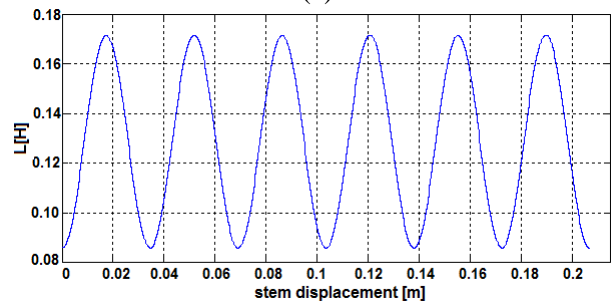
Considering the equivalent circuit of each coil, physical operating principle is described by relationship (6) and the block diagram in Fig. 14.

$$\varepsilon_i(t) = \left(R_{\text{int}} + R_{ext}\right)\cdot i(t) + L(t)\frac{di}{dt} \quad (6)$$

Where R_{int} is the resistance of the coil itself, R_{ext} is the external resistance (load connected to the damper), $L(t)$ is the inductance and $i(t)$ is the current.

(a)

(b)

Fig. 13: flux (a) and inductance (b) variation of each coil (sector) as a function of the stem displacement.
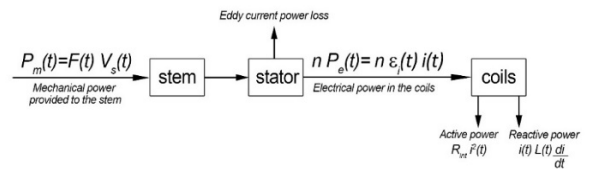

Fig. 14: Block diagram of the energy balance.

Electric power provided to the coils can be obtained multiplying the terms of the relationship (5) by the current $i(t)$. The force applied to the stem and the damping coefficient of the device can be determined by:

$$C_d(t) = \frac{n\,\varepsilon_i(t)\,i(t)}{V_S^2(t)} \quad (7)$$

WSEAS TRANSACTIONS on SYSTEMS

Cannizzaro L., Virzi' Mariotti G.,
Giallanza A., Porretto M., Marannano G.

considering the diagram of the energy balance in Fig. 14. The mathematical model, implemented in Matlab-Simulink environment [37], allows analyzing the damper working by varying the input data. Fig. 15 shows the complete block scheme. The first two blocks named *From Workspace* represent the input quantities that are recalled by Workspace of Matlab, they are the electromotive force and the circuit inductance, depending on the time.
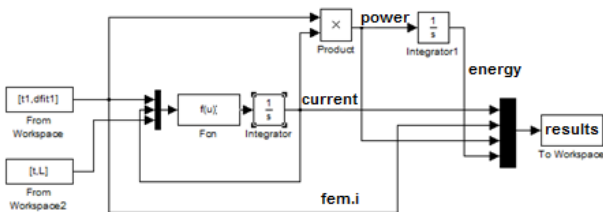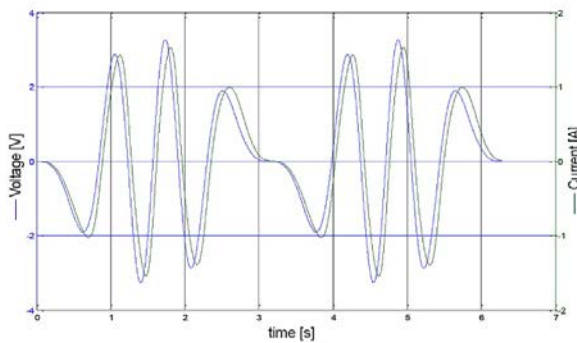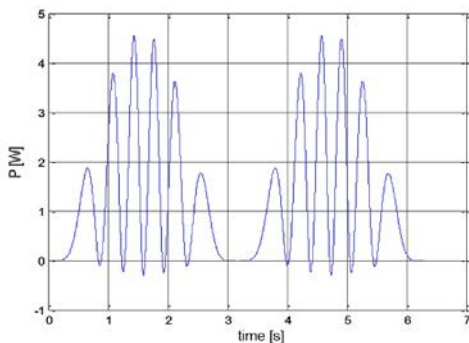

Fig. 15 – complete block scheme in Simulink

(a)

(b)

Fig. 16: (a) Current and voltage trends; (b) power trend in each coil.

The third input quantity is the resistance that does not depend on the time and is inserted into the block *Fcn*, also recalling it by Workspace of Matlab. The adopted resolver is ODE 45. The current values versus the time are reported to Workspace by the block *To Workspace*. The variation law of the induced electromotive force and the relative current in each coil are obtained defining the spire number of the coils and the external load resistance. At last the values of power and energy are exported to

Workspace; of course this procedure calls for a Mat-file program. The first analysis was carried out considering zero the value of the external load resistance, so that the coils are short-circuited. One can demonstrate that the value of the damping coefficient is not function of the number of turns of the coils. The current and the voltage trends (Fig. 16a), the power trend (Fig. 16b) and, finally, the value of the damping coefficient (Fig. 17) are obtained imposing a sinusoidal translation speed of the stem. Fig. 16a also shows the phase displacement between voltage and current.
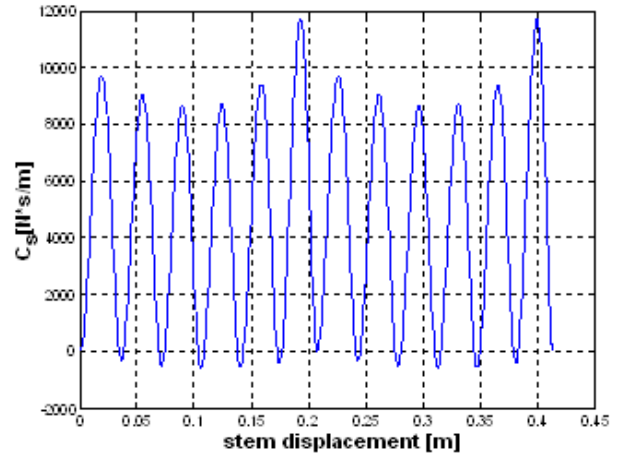

Fig. 17: Damping coefficient versus the stem displacement (short-circuited coils).
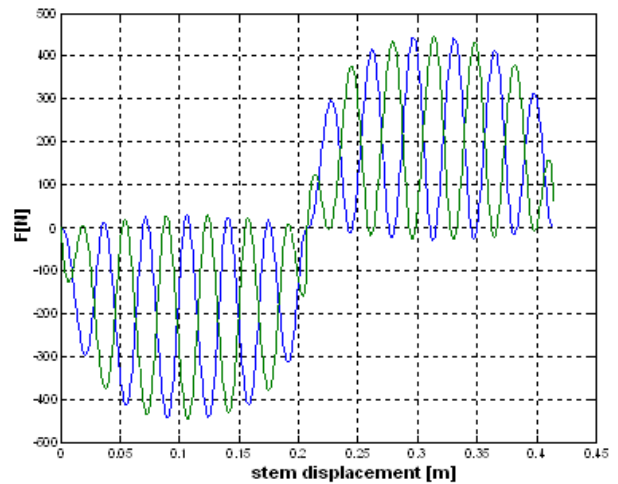
Fig. 18: Force generated by the two blocks of coils versus the stem position.

Fig. 17 shows that the damping coefficient strongly depends on the stem position; in particular, the trend for two successive strokes of the stem is reported (outward stroke and return stroke). Moreover the shape of the damping coefficient curve indicates that the studied device could not be appropriate for the automotive suspension systems. In fact, the damping coefficient should be as much as possible constant with the stem position. Then the stator

WSEAS TRANSACTIONS on SYSTEMS

Cannizzaro L., Virzi' Mariotti G.,
Giallanza A., Porretto M., Marannano G.

geometry is modified so that the effect of the coils in terms of force to the stem is out of phase, optimizing the device. The phase-shift is implemented shifting a block of 10 coils by an amount equal to the half-pitch of the magnets, according to the direction of the stem. In this way, the concatenated magnetic flux is phase-shifted by 90 degrees. Fig. 18 shows the trend of the force generated by the two blocks of 10 coils versus the distance covered by the stem (forward stroke and return stroke), so that the damping coefficient assumes a more stable trend around its mean value (Fig. 19).
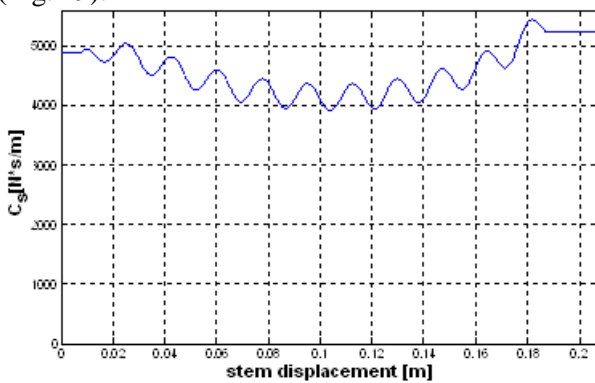

Fig. 19: Damping coefficient versus the stem displacement (optimized solution with short-circuited coils).
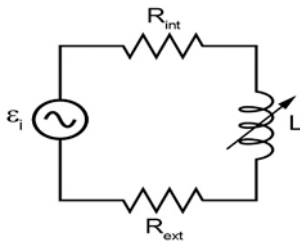

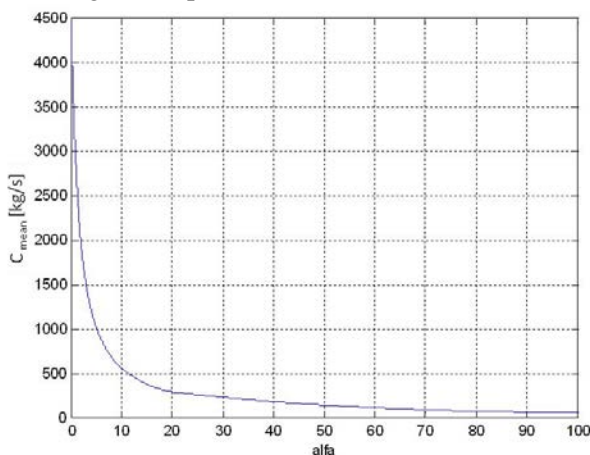Fig. 20: Equivalent circuit of each coil.

Fig. 21: Mean damping coefficient versus α ratio.

In order to harvesting the energy produced by the damper, the coils have to be connected to an electric energy storage system. Fig. 20 shows the equivalent circuit of each coil, since the storage system can be assimilated to a resistive load. The harvested power is equal to $P_{acc}(t) = R_{ext} \cdot i(t)^2$. The introduction of an external load causes electric current decrease and reduction of the forces applied to the stem, given that the forces are related to interaction between magnetic field and electric current. The mean damping coefficient appears strongly dependent on the resistance ratio $\alpha = \dfrac{R_{ext}}{R_{int}}$. In fact the mean damping coefficient decreases increasing the value of the external resistance, as Fig. 21 shows.

The damper/generator efficiency is given by:

$$\eta = \frac{P_{acc}}{P_{gen}} = \frac{P_{acc}}{P_{diss} + P_{acc}} = \frac{R_{ext}i^2}{R_{int}i^2 + R_{ext}i^2} = \frac{R_{ext}}{R_{int} + R_{ext}} = \frac{\alpha}{1+\alpha} \qquad (8)$$

The efficiency versus α ratio is shown in Fig. 22:
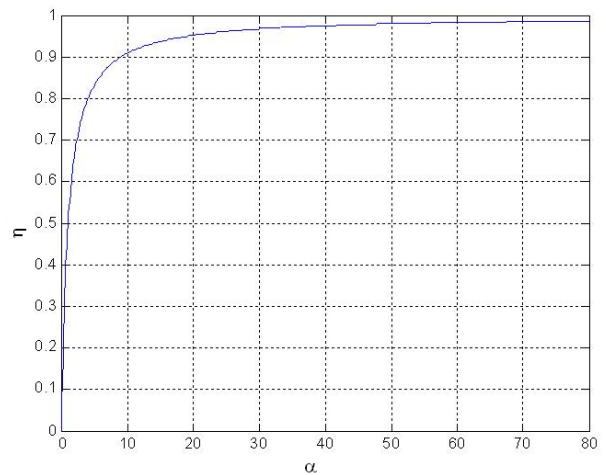
Fig. 22: Efficiency trend versus α ratio.

High damping coefficient needs a low value of external resistance and a low value of accumulation power. In this paper the hypothesis is done that the damper is installed on an electric car with a mass of m_{tot}=800kg, with the only purpose to illustrate the procedure.

Considering the mass on each wheel about m=200kg and assuming a simplified model of one degree of freedom suspension, the optimal damping coefficient [30] [38] is obtained by:

$$C_{opt} = \sqrt{\frac{k \cdot m}{2}} = 1566 \, Ns/m \qquad (9)$$

where the spring constant is obtained by relationship (10) assuming that the spring compression is Δx=80mm, under static load:

$$k = \frac{mg}{\Delta x}..[N/m] \qquad (10)$$

WSEAS TRANSACTIONS on SYSTEMS

Cannizzaro L., Virzi' Mariotti G.,
Giallanza A., Porretto M., Marannano G.

and neglecting the constant of the tire. Fig. 19 shows that the damping coefficient is not perfectly constant versus the steam position, but has some fluctuation around the mean value. In order to avoid lower values than the optimal, the damping coefficient C_{opt} is increased of 12% about, so that it assumes the value C_{opt}=1750 Ns/m corresponding to $\alpha = 2.35$. Its trend versus the stem position is reported in Fig. 23: the damping coefficient fluctuations are lower than those of the short circuit case. The power dissipated by the damper (or, in this case, the power converted into electrical energy) is dependent on the road surface irregularities and on the car speed. These results are in very good qualitative agreement with the works [8] [27]
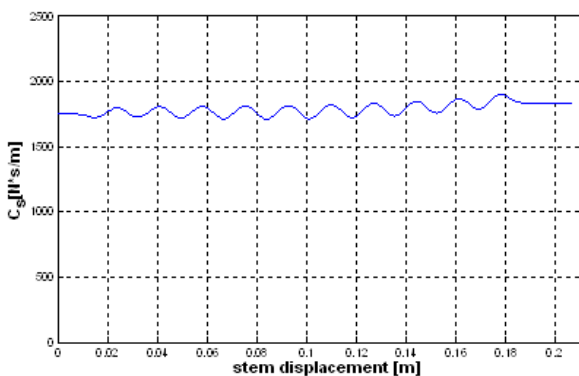

Fig. 23: Damping coefficient versus the stem position (optimized solution with coils connected to an electric storage system).

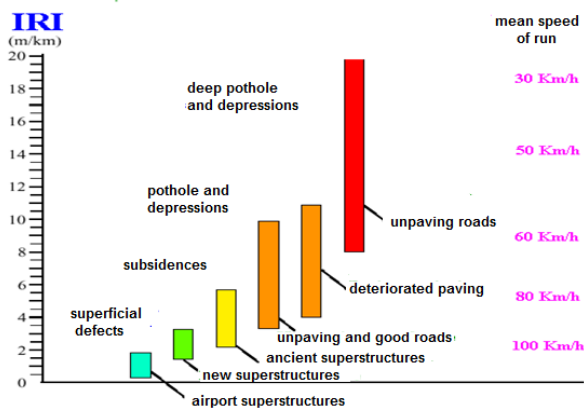# 4 Electric power recovered by the suspension

Fig. 24 – Roughness index

4.1 The Roughness index

The road irregularities are defined as the shifting of the ground surface from an ideal reference plane and are characterized by: wave length λ in longitudinal direction, roughness width h and irregularity index:

$$IRI = \frac{h}{\lambda} \qquad (11)$$

IRI (International Roughness Index) (Fig. 24) [39]is a mathematic representation of the suspension rebound during the road run. The run speed equal to 80 km/h, the road length equal to 1 km and the ratios among stiffness, mass, damper and shaking are established by the rules [40] in the following way: Ks/M=63.3s^{-2}, Cs/M=6s^{-1}, m/M=0.15, Kt/M =653s^{-2}, where Ks, M, Cs, m, Kt indicate respectively the elastic constant of the spring, the sprung mass, the damper constant, the unsprung mass, the tire elastic constant. IRI is influenced in particular way by the wave length between 1 and 30 m, corresponding to frequency 0.03 and 0.8 cycles/m respectively.

Roads with greater IRI values than 8m/km are quasi impracticable also at low speed, IRI = 0 represent a perfectly plane and smooth surface.

4.2 Calculation and comparison

Choosing IRI=3m/km [41] and a car speed equal to v=80 km/h, for a profile width h=0.03 m, the λ value is equal to 10 m by relationship (11). The oscillation frequency of the suspension is equal to:

$$f = \frac{v}{\lambda} = 2,22 \ [Hz]; \quad \omega = 2\pi f = 13,95 \qquad (12)$$

Inserting the pulsation value in Matlab mathematical model and considering the stem stroke equal to 2h, the total electric power in the coils is obtained. Fig. 25 shows the trend versus the time.

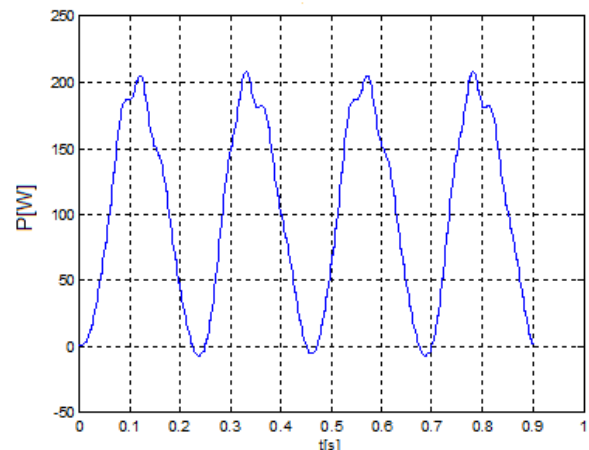Fig. 25: Generated power by the damper (20 coils)

the mean value of the generated power in Fig. 25 is equal to:

$$P_{mg} = 102,4 \ [W] \qquad (13)$$

Assuming α=2.35, the efficiency value is equal to 0.7 by (8). Then the power is partly accumulated:

$$P_{acc} = P_{mg}\eta = 71,8 \ [W] \qquad (14)$$

and partly dissipated due to the Joule effect:

$$P_{diss} = P_{mg}(1 - \eta) = 30.6 \ [W] \qquad (15)$$

WSEAS TRANSACTIONS on SYSTEMS

Cannizzaro L., Virzi' Mariotti G.,
Giallanza A., Porretto M., Marannano G.

Considering all four damper of the car, the harvested power is finally equal to:

$$P_{tot} \approx 280 \, [W] \qquad (16)$$

Table 2 shows the comparison of the harvested power with other works in literature. Results show that the proposed damper is suitable for the successive investigations and the experimentation. The results are encouraging, although the harvesting efficiency highly depends on the road conditions; a more effective comparison should be executed with analogous parameters (IRI, *v*, *h*).

Table 2- Comparison with harvesting energy for other similar dampers in literature

Ref.	Harv. Energy	Other indications
[14]	68W (mean 19W)	v=48 km/h
[26]	88.8 W	η=21%
[9]	21.13 W	
[10]	100-400W	v=60mph
[11]	90 W	h=0.03 m
[12]	200 W	10 Hz 3 mmexcit.
[4]	200-300W	Temp. less 130°C
This	280 W	v= 80km/h h=0.03m

5 Conclusions

An electromagnetic regenerative damper for automotive applications is studied in this paper. Today the vehicle construction needs electromechanical devices, to increase not only the driving comfort but also safety and performances. The main purpose of vehicles manufacturers is the optimization of each component, aiming at the reductions of fuel consumption and pollutant and at the increment of the efficiency. The innovative suspension system, constituted by an electromagnetic damping system, allows harvesting energy, which the traditional shock absorbers dissipate in heat. The use of rare-earth permanent magnets allows designing electric machines with high values of power that were not possible to reach until short time ago. A shock absorber, constituted by a permanent magnet linear generator, is designed and optimized, but the choice of the material cannot be considered definitive, because the Supermendur is expensive and is found with difficulty; another ferromagnetic material can be chosen determining experimentally its magnetization curve, or by the literature. The mathematical model is implemented in Matlab-Simulink environment, obtaining the main operating parameters. Moreover, the magnetic field and flux values, analytically calculated, are in

very good agreement with the values by FE analysis.

One can observe that the damping curve is strongly dependent on the external load resistance value. The regulation of the suspension damping behavior can be obtained by the modulation of the harvesting system. The electromagnetic damper is, therefore, semi-active and the damping coefficient variation is achieved by varying the external load value. The maximum comfort behavior is obtained with high load resistance and then with high value of harvested power. The rigid behavior is obtained with low value of the external load resistance, when the system accumulates energy at low power. Finally the main advantages of an electromagnetic suspension are:

- To contribute at the increment of the range autonomy (the main barrier for the commercial success of electric or hybrid vehicles);
- To increase the road performances because the electromagnetic damper is semi-active, by varying its damping behavior by means of an electronic control system.
- The weight of the designed shock absorber, obtained by CAD system, is not very greater than the traditional damper.

The work shows that a semi-active automotive suspension system can provide significant benefits. A semi-active suspension has the advantage of using negligible energy and that the damping coefficient of the shock absorber is changed in real time. By the harvesting energy view point, the presented device has the vantage to obtain a rather high power. The results suggest that the IRI number (road roughness, tire stiffness, vehicle driving speed) has great influence to the harvesting power potential.

The device present a disadvantage: if the oscillating frequencies of the rod are increased, the effects of the auto induction are more and more evident and the trend of the damping coefficient versus the rod position is more and more unstable around its mean value, with negative effects on the passengers comfort. Another disadvantage is the high cost of implementation regard to a normal viscous damper. For the practical application the advantages of the energy recovery have to justify the greater cost of the entire system. Possible developments of this work are:

- the dynamic analysis of the suspension to study the acceleration effects due to the damping coefficient variation, in order to optimize the device to reach constant the damping coefficient.

WSEAS TRANSACTIONS on SYSTEMS

Cannizzaro L., Virzi' Mariotti G.,
Giallanza A., Porretto M., Marannano G.

- The cost may be reduced using another ferromagnetic material, less expensive and easily found.

References

[1] Kruckemeyer W. C., Buchanan H. C. Jr., Fannin W. V., Rotational actuator for vehicle suspension damper, *U.S. Patent 4 644 200*, Feb. 17, 1987.

[2] Beno J. H., Weeks D. A., Weldon W. F., Constant force suspension, near constant force suspension, and associated control algorithms, *U.S. Patent 5 999 868,* Dec. 7, 1999.

[3] Cassidy I. L., Scruggs J. T., Behrens S., Design of electromagnetic energy harvesters for large-scale structural vibration applications, *Proc. SPIE 7977 Active and Passive Smart Structures and Integrated Systems* (2011). doi:10.1117/12.880639.

[4] Amati N., Festini A., Tonoli A., Design of electromagnetic shock absorbers for automotive suspensions, *Vehicle System Dynamics: International Journal of Vehicle Mechanics and Mobility* (2011), 49 (12), 1913-1928. doi:10.1080/00423114.2011.554560.

[5] Song X., Li Z., Edmondson J. R., Regenerative passive and semi-active suspension *US Patent Specification* 7087342 B2 (2006).

[6] Tang X., Zuo L., Simulation and experiment validation of simultaneous vibration control and energy harvesting from buildings via tuned mass dampers, *Proceedings of the 2011 American Control Conference*, San Francisco, USA (2011).

[7] Zhang Y., Huang K., Yu F., Gu Y., Li D., Experimental verification of energy-regenerative feasibility for an automotive electrical suspension system, *Vehicular Electronics and Safety, 2007. ICVES.IEEE International Conference on, Beijing* (2007).doi: 10.1109/ICVES.2007.4456407.

[8] Singal K., Rajamani R., Simulation study of a novel Self-powered active suspension system for automobiles, (2011) *American control conference,* San Francisco, USA, June 29-July 01, 2011, pp. 3332-3337

[9] Zaouia M.; Benamrouche N.; Djerdir A., Study and analysis of an Electromagnetic Energy Recovery Damper (EERD) for automotive applications, *Electrical Machines (ICEM), 2012 XXth International Conference* pp2716 - 2721, DOI: 10.1109/ICElMach.2012.6350270

[10] Zuo L., Zhang P. S., Energy Harvesting, Ride Comfort, and Road Handling of Regenerative Vehicle Suspensions *J. Vib. Acoust* 135(1), 011002 (Feb 04, 2013) (8 pages) Paper No: VIB-11-1060; doi: 10.1115/1.4007562.

[11] Sultoni A. I., Sutantra I N, Pramono A. S., Vibration Energy Harvesting on Vehicle Suspension Using Rotary and Linear Electromagnetic Generator, IPTEK, *The Journal for Technology and Science,* Vol. 24, No. 1, April 2013.

[12] Zhigang Fang, Xuexun Guo, Lin Xu, Han Zhang, Experimental Study of Damping and Energy Regeneration Characteristics of a Hydraulic Electromagnetic Shock Absorber, *Advances in Mechanical Engineering*, Volume 2013, Article ID 943528, 9 pages, http://dx.doi.org/10.1155/2013/943528.

[13] Yin J., Chen X., Li J., Wu L., Investigation of Equivalent Unsprung Mass and Nonlinear Features of Electromagnetic Actuated Active Suspension, *Shock and Vibration* (2015), doi: 10.1155/2015/624712.

[14] Li Z., Zuo L., Luhrs G., Lin L., Qin Y., Electromagnetic Energy-Harvesting Shock Absorbers: Design, Modeling, and Road Tests. *IEEE transactions on vehicular technology* (2013), 62(3), 1065-1074.doi: 10.1109/TVT.2012.2229308.

[15] Suda Y., Shiba T., New hybrid suspension system with active control and energy regeneration, *Vehicle System Dynamics: International Journal of Vehicle Mechanics and Mobility* (1996), 25(1), 641-654. doi: 10.1080/00423119608969226.

[16] Suda Y., Nakadai S., Nakano K., Hybrid suspension system with skyhook control and energy regeneration (Development of self-powered active suspension), *Vehicle System Dynamics: International Journal of Vehicle Mechanics and Mobility* (1998), 29(1), 619–634. doi: 10.1080/00423119808969590.

[17] Nakano K., Combined type self-powered active vibration control of truck cabins, *Vehicle System Dynamics: International Journal of Vehicle Mechanics and Mobility* (2004), 41(6), 449-473. doi: 10.1080/00423110512331383858.

[18] Szabò L., Oprea C., Viorel I., Biró K., Novel permanent magnet tubular linear generator for wave energy, *IEEE International Electric Machines and Drives* (2007), 983-987. doi: 10.1109/IEMDC.2007.382809.

[19] Ivanova I., Agren O., Bernhoff H., Leijou M., Simulation of cogging in a 100 kW permanent magnet octagonal linear generator for ocean wave conversion, *Underwater Technology*

WSEAS TRANSACTIONS on SYSTEMS

Cannizzaro L., Virzi' Mariotti G.,
Giallanza A., Porretto M., Marannano G.

(2004), 345-348. doi: 10.1109/UT.2004.1405602.

[20] Leijon M., Danielsson O., Eriksson M., Thorburn K., Isberg J. et al., An electrical approach to wave energy conversion, *Renewable Energy* (2006), 31(9), 1309-1319. doi: 10.1016/j.renene.2005.07.009

[21] Oprea R. A., Mihailescu M., Chirila A. I., Deaconu I. D., Design and Efficiency of Linear Electromagnetic Shock Absorbers, *Optimization of Electrical and Electronic Equipment* (OPTIM) (2012), 630-634. doi: 10.1109/OPTIM.2012.6231813.

[22] Nagode C., Ahmadian M., Taheri S., Effective energy harvesting devices for railroad applications. *Active and Passive Smart Structures and Integrated Systems* (2010).doi: 10.1117/12.847866.

[23] Zuo L., Scully B., Shestani J., Zhou Y., Design and characterization of an electromagnetic energy harvester for vehicle suspensions, *Smart Materials and Struct*ures (2010), 19, 1-10.

[24] Tang X., Lin T., Zuo L., Design and Optimization of a Tubular Linear Electromagnetic Vibration Energy Harvester, *IEEE/ASME Transactions on Mechatronics* (2013), 615 – 622. doi: 10.1109/TMECH.2013.2249666.

[25] Ebrahimi B., Khamesee M.B., Golnaraghi F., Permanent magnet configuration in design of an eddy current damper, *Microsystem Technologies* (2010), 16, 19-24. doi: 10.1007/s00542-008-0731-z.

[26] Gupta A., Jendrzejczyk J. A., Mulcahy T. M., Hull J. R., Design of electromagnetic shock absorbers, *Int J Mech Mater Des* (2006) 3:285–291, DOI 10.1007/s10999-007-9031-5

[27] Kim Y.-B., Hwang W.-G., Kee C.-D., Yi H.-B. Active vibration control of a suspension system using an electromagnetic damper, *Proc Instn Mech Engrs* Vol 215 Part D, 2001 215: 865, DOI: 10.1243/0954407011528446

[28] Barbaraci G.; Virzi' Mariotti G., Influence on The Dynamic Behaviour of Full Car Equipped by Magnetorheological Damper via Switch On/Off and H∞ Controller – *23th JUMV International Automotive Conference*, Belgrade, Serbia, 19-21 April 2011

[29] Barbaraci, G; Virzi' Mariotti, G. - The Recovery of the Optimal Damping Constant by the MRF Damper, *Mobility and Vehicle Mechanics,* RS, vol. 35, n. 4, December 2009, pp. 1-17, ISSN: 1450-5304

[30] Sapinski B., Experimental study of a self-powered and sensing MR-damper-based

vibration control system, *Smart Materials and Structures,* 20, (2011) 105007 (13pp)

[31] Snamina J., Sapinski B., Energy balance in self-powered MR damper-based vibration reduction system, *Bulletin of the Polish Academy of Sciences Technical Sciences,* vol. 59, No 1, 2011, DOI:10.2478/v10175-011-0011-4

[32] Bissal A., Salinas E., Magnusson J., Engdahl G., On the Design of a Linear Composite Magnetic Damper, *IEEE Transactions on magnetics* (2015), 51(11). doi: 10.1109/TMAG.2015.2440770.

[33] Barbaraci G., Virzi' Mariotti G., Porretto M., Studio di un ammortizzatore elettromagnetico a recupero di energia, *42° Convegno AIAS,* 11-14 September 2013, Salerno, Italy.

[34] Cannizzaro L., Virzi' Mariotti G., Giallanza A., Porretto M., Marannano G., Design of an Electromagnetic Regenerative Damper and Energy Harvesting Assessment, *Journal of Electromagnetics,* (2016),**1**, 5-11

[35] Barbaraci G., Marannano G., Virzi' Mariotti G., Analysis of the Effects of Magnetic Field on the Induced Stress in Drilled Plates – *International Journal of Solid and Structures* – on line 18/1/2013, http://dx.doi.org/10.1016/j.bbr.2011.03.031, 50, 9 (2013) 1425–1436.

[36] Goldman A., *Handbook of Modern Ferromagnetic Materials,* Kluwer Academic Publishers, New York, 1999.

[37] Klee H., Allen R., *Simulation of dynamic systems with Matlab and Simulink*, CRC Press, II ed., London, (2011), ISBN 978-1-4398-3673-6.

[38] Virzi' Mariotti G. – Some Observations on the Best Damping Constant - *XVIII Science and Motor Vehicles 2001* - Belgrade, 28-30 May 2001

[39] Sayers, M. W., Gillespie, T. D., and Queiroz, C. A. V., The International Road Roughness Experiment: Establishing Correlation and a Calibration Standard for Measurements, *World Bank Technical Paper* No. 45, The World Bank, Washington DC, 1986.

[40] ASTM E1926 - *08 Standard Practice for Computing International Roughness Index of Roads from Longitudinal Profile Measurements*.

[41] Coni M., Silanos G., Annunziata F., Le vibrazioni indotte dalle irregolarità superficiali del profilo stradale, *Convegno Nazionale Traffico e Ambiente, Trento* (Italy) (2000).